Table I. Extended Hückel Parameters

atom	orbital	H_{ii} (eV)	ζ
H	1s	-13.6	1.30
C	2s	-21.4	1.63
	2p	-11.4	1.63
Si	3s	-17.3	1.38
	3p	-9.2	1.38
B	2s	-15.2	1.30
	2p	-8.5	1.30
Al	3s	-12.3	1.17
	3p	-6.5	1.17
Ga	4s	-14.5	1.77
	4p	-7.8	1.55

imentally. We would be more than rewarded if this work can stimulate further research in that direction.

Acknowledgment. Y.-T.W. dedicates this paper to Professor Ruslan Minyaev, with gratitude for his inspiration and encouragement. Our work was carried out with the support of the Office of Naval Research. Acknowledgement is also made to Jane Jorgensen and Elisabeth Fields for their expert drawings.

Appendix

All calculations are performed by the extended Hückel method within the tight-binding formalism.[18,19,47,48] The distance-dependent k

$$k = 1 + (\kappa + \Delta^2 - \Delta^4\kappa) \exp(-\delta(r - d_o))$$

$$\kappa = 0.80 \qquad \Delta = (H_{ii} - H_{jj})/(H_{ii} + H_{jj}) \qquad \delta = 0.13$$

and the two-body repulsions have been explained in a previous paper.[23] The extended Hückel parameters are listed in Table I. The k points are generated according to the geometrical method of Böhm and Ramirez.[49]

Registry No. Si, 7440-21-3; B, 7440-42-8.

(47) Ammeter, J. H.; Bürgi, H.-B.; Thibeault, J. C.; Hoffmann, R. *J. Am. Chem. Soc.* **1978**, *100*, 3686.
(48) Whangbo, M.-H.; Hoffmann, R. *J. Am. Chem. Soc.* **1978**, *100*, 6093.
(49) Ramirez R.; Böhm M. C. *Int. J. Quantum Chem.* **1986**, *30*, 391.

Electron Distributions in Peptides and Related Molecules. 2. An Experimental and Theoretical Study of (*Z*)-*N*-Acetyl-α,β-dehydrophenylalanine Methylamide

Mohamed Souhassou,[†] Claude Lecomte,*[,†] Nour-Eddine Ghermani,[†,§] Marie Madeleine Rohmer,[‡] Roland Wiest,[‡] Marc Benard,*[,‡] and Robert H. Blessing[†,∥]

Contribution from the Laboratoire de Minéralogie-Cristallographie, URA CNRS 809, Université de Nancy I, Faculté des Sciences, B.P. 239, 54506 Vandoeuvre les Nancy Cedex, France, and the Laboratoire de Chimie Quantique, UPR 139 du CNRS, Université Louis Pasteur, 4 rue Blaise Pascal, 67000 Strasbourg, France. *Received June 19, 1991*

Abstract: The crystal structure, thermal vibrations, and electron density of (*Z*)-*N*-acetyl-α,β-dehydrophenylalanine methylamide have been analyzed using single-crystal X-ray diffraction data measured at 100 K with Mo Kα radiation to a resolution corresponding to $(\sin\theta_{max})/\lambda = 1.35$ Å^{-1}. Averaging equivalent data among the 14666 reflections measured gave 7324 unique data [$R_i(F^2) = 0.016$]. A multipolar atomic density model was fitted against the 6035 unique data with $I > 3\sigma(I)$ [$R(F) = 0.022$, $R_w(F) = 0.018$] in order to calculate phases for the crystal structure factors and map the valence electron distribution. Ab initio SCF calculations have been carried out at the crystallographic molecular geometry with two basis sets. The density maps obtained with a medium-size basis set (double-ζ quality for the valence shell of all atoms) agree qualitatively with the experimental static model maps. Near quantitative agreement between theory and experiment is obtained with an extended basis set (triple-ζ plus polarization quality for the valence shell of all atoms, except those belonging to the methyl and phenyl substituents). Crystal data: $C_{12}H_{14}O_2N_2$, $M_r = 218.32$; monoclinic *Cc* from 295 to 100 K; at 100 K $a = 10.193$ (1), $b = 15.115$ (1), and $c = 8.561$ (2) Å, $\beta = 121.13$ (2)°, $V = 1129$ Å^3, $Z = 4$, $\rho_x = 1.28$ g cm^{-3}, μ(Mo Kα) = 0.9 cm^{-1}, $F(000) = 464$ electrons.

Introduction

The proper description of electrostatic properties of small peptides and pseudopeptides is of considerable importance for our understanding of molecular recognition processes and for the design of new drugs. As part of our program[1,2] to map the electron distribution and to calculate the electrostatic properties of peptides we have already studied *N*-acetyl-L-tryptophan methylamide[3] and Leu-enkephalin, for which a preliminary report has been published.[4] In our study of *N*-acetyl-L-tryptophan methylamide[3] we have obtained a reasonable agreement between experimental and theoretical deformation density maps, within the limitations im-

Chart I

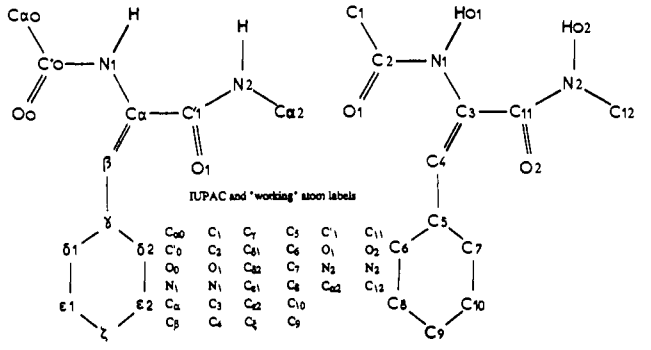

* Authors to whom correspondence should be addressed.
† Université de Nancy I.
‡ Université Louis Pasteur.
∥ Permanent address: Medical Foundation of Buffalo, 73 High Street, Buffalo, NY 14203.
§ Permanent address: Laboratoire de Physique du Solide et des Couches Minces, Faculté des Sciences, Université Cadi Ayyad, BP 515, Marrakech, Morocco.

0002-7863/92/1514-2371$03.00/0

Table I. Least Squares Refinement Statistics of Fit[a]

refinement	cutoff $s = \sin\theta/\lambda$, Å^{-1}	R, %	wR, %	S	K	n	m	type
I	$0.9 < s < 1.35$, $I > 0$	7.89	5.30	0.85	0.6849	3397	143	spherical
II[b]	$0.9 < s < 1.35$, $I > 0$	10.50	6.04	0.90	0.6998	3397	143	spherical
III[c]	$s \leq 0.9$, $I > 3\sigma(I)$	2.84	4.04	2.42	0.6959	3032	57	spherical
IV	$s < 1.35$, $I > 3\sigma(I)$	3.74	4.54	2.05	0.6995	6035	1	spherical
V	$s < 1.35$, $I > 3\sigma(I)$	2.19	1.85	0.85	0.6887	6035	423	multipolar
VI[d]	$s \leq 0.9$, $I > 3\sigma(I)$	1.28	1.37		0.6887	3032	0	multipolar

[a] $\chi^2 = \sum w(|F_o| - K|F_c|)^2$, $w = \sigma^2(|F_o|)^{-1}$; $R = \sum||F_o| - K|F_c||/\sum|F_o|$; $wR = (\chi^2/\sum w|F_o|^2)^{1/2}$; $S = [\chi^2/(n-m)]^{1/2}$; n data and m parameters. The values of $S < 1$ indicate a slight overestimation of the experimental errors as explained in ref 3. [b] Refinement against I(H), other refinements are made against F(H). [c] Hydrogen atoms refinement only. [d] Structure factor calculation only, not refinement.

posed by the split-valence-basis quantum chemical approximations and by the crystallographic thermal motion convolution and finite resolution. We have concluded that "more detailed comparison requires polarization functions and high resolution static density maps from the experimental data". To make such a comparison we have selected an α,β-dehydro monopeptide, (Z)-*N*-acetyl-α,β-dehydrophenylalanine methylamide, which crystallizes as high-quality single crystals for which we could expect very high resolution X-ray data (see Chart I).

Furthermore, synthetic research on dehydro peptides has considerably increased during the last 5–10 years because of their use as new drugs.[5-9] The α,β-dehydro residues are able to fix the orientation of a side chain while they reduce enzymatic degradation.[9] However, except for some antibiotic peptides, very few theoretical studies[10,11] have been devoted to these pseudopeptides, and no high-resolution X-ray data are available.

The present paper reports the electron distribution of (*Z*)-*N*-acetyl-α-β-dehydrophenylalanine methylamide (hereafter, *N*-AcΔPhe-NHMe) obtained from a high-resolution Mo Kα X-ray experiment [$s_{max} = (\sin\theta/\lambda)_{max} = 1.35$ Å^{-1}] compared with two ab initio SCF calculations. The first calculation was done with a medium basis set (double-ζ quality for the valence shells of all atoms), while the second corresponds to an extended basis set (triple-ζ plus polarization for the valence shell of all atoms, except those belonging to the methyl and phenyl substituents). Some preliminary results on the experimental density and double-ζ calculations were already reported.[12]

Experimental Work

Crystallographic Analysis. (a) Data Collection. *N*-AcΔPhe-NHMe was obtained from G. Boussard and M. Marraud[13] and recrystallized from a solution of ethanol–ethyl acetate by solvent evaporation. A crystal of 0.32 × 0.30 × 0.28 mm was used to measure Mo Kα X-ray diffraction data on an Enraf Nonius CAD4 diffractometer equipped with a liquid nitrogen vapor stream apparatus and installed in a drybox to prevent ice formation on the crystal. The gas stream temperature was maintained at 100 ± 3 K as monitored by a copper–constantan thermocouple positioned ~5 cm upstream from the crystal. The homogeneity of the beam from the graphite incident beam monochromator was measured, and the intensity varied by less than 2.9% over the area intercepted by the specimen crystal. Lattice parameters were obtained by least squares fit to the optimized setting angles of the $K\alpha_1$ peaks of 25 reflections with $28° < 2\theta < 47°$ and are given in the abstract. Intensity data were recorded as ω–2θ scan profiles to a resolution of $s = (\sin\theta)/\lambda = 1.35$ Å^{-1} for a total of 14 666 reflections in the following way: For $s < 0.5$ Å^{-1} three symmetry equivalents, and for $0.5 < s < 1$ Å^{-1} two equivalents, were measured. After a conventional refinement against the low-order data ($s < 0.9$ Å^{-1}), high-angle data were calculated to $s = 1.35$ Å^{-1}, and for those with an estimated $I > 4\sigma(I)$, two equivalents were measured. During the data collection, seven standard reflections, 800, $\bar{8}00$, 060, $\bar{5}\bar{5}6$, $5\bar{5}6$, $\bar{5}5\bar{6}$, and $0\bar{6}0$, were measured at 4-h intervals. The total $\Delta\omega$ (deg) scan width was $1.35 + 0.35 \tan\theta$ with a constant detector aperture of 6 × 4 mm. A prescan speed $v = (d\omega/dt)$ of 3.5° min^{-1} and a final scan speed depending on the signal-to-noise ratio ($0.5 < v < 3.5°$ min^{-1}) were used. The total exposure time of the sample was 690 h. During the whole experiment (~7 weeks), no temperature, crystal, or diffractometer problems occurred.

(b) Data Processing. Data reduction and error analysis were done using the programs of Blessing.[14,15] Reflection integration limits were from a Lorentzian model for the peak width variations. A polynominal fit to the smooth decline of ~3.5% in the standard reflection intensities over the 690 h of X-ray exposure was used to scale the data and to derive the instrumental instability coefficient $p = 0.0065$ for the calculation of $\sigma^2(|F|^2) = \sigma_c^2(|F|^2) + (p|F|^2)^2$ with σ_c^2 from propagation of error calculations in which counting statistics and scan angle setting uncertainties [$\sigma(\omega) = 0.005°$] made the most important contributions. The excellent small value of p over the 7-week period of data collection shows that large data sets can be measured very precisely given sufficient diffractometer time. Absorption corrections and beam inhomogeneity corrections were deemed unnecessary. Averaging equivalent measurements gave 7324 unique data of which 6035 had $I > 3\sigma(I)$. Internal agreement indices were $R = 0.016$ and $R_w = 0.025$ for all data, and 0.012 and 0.016 for the 571 data with $s < 0.5$ Å^{-1}, where $R_w = [\sum w(|F|^2 - \langle|F|^2\rangle)^2/\sum w(|F|^2)^2]^{1/2}$, $w = 1/\sigma^2(|F|^2)$ and $R = R_w$ if $w = 1$.

(c) Least Squares Refinements. The room temperature crystal structure was known from an earlier study.[13] Since very good quality high-order data were available, the high-order refinement of the C, N, O atoms was made against the 3397 reflections with $s = (\sin\theta/\lambda > 0.9$ Å^{-1} and $I > 0$. Refinements against the $|F|$ (refinement I) and $|F|^2$ (refinement II) data led essentially to the same x, y, z, U^{ij} parameters within 1σ. Statistics of fit are given in Table I. Hydrogen atoms were found by difference Fourier synthesis ($s < 0.9$ Å^{-1}) and refined isotropically against the low-order data [refinement III, Table I], and then their coordinates were adjusted by extending along the C–H bond and N–H bond directions to bond lengths of 1.07 Å C–H and 1.03 Å N–H, equal to average values from neutron diffraction.[16] The bound atom form factor for hydrogen from Stewart, Davidson, and Simpson,[17] the form factors for the non-hydrogen atoms calculated from Clementi and Raimondi[18] wave functions, and the real and imaginary anomalous dispersion corrections to the form factors given by Cromer[19] were used in the structure factor calculations.

Because the structure is noncentrosymmetric, it is necessary to have very accurate phases for the structure factors in order to get reliable

(1) Lecomte, C.; Souhassou, M.; Ghermani, N.; Pichon-Pesme, V.; Bouhmaida, N. *Trans. Am. Cryst. Assoc.* **1990**, *26*, 52–76 (electron densities symposium).
(2) Lecomte, C.; Pichon-Pesme, V.; Ghermani, N.; Souhassou, M. *J. Mol. Struct.*, THEOCHEM, in press.
(3) Souhassou, M.; Lecomte, C.; Blessing, R. H.; Aubry, A.; Rohmer, M. M.; Wiest, R.; Benard, M.; Marraud, M. *Acta Crystallogr.* **1991**, *B47*, 253–266.
(4) Pichon-Pesme, V.; Ghermani, N.; Lecomte, C. *Abstracts, 40th American Crystallographic Association Meeting, New Orleans, April* **1990**, *18*, 78.
(5) Yosioka, H.; Aoki, T.; Goko, H.; Nakatsu, K.; Noda, T.; Sakakibara, H.; Take, T.; Nagata, A.; Abe, J.; Wakamiya, T.; Shiba, T.; Kaneko, T. *Tetrahedron Lett.* **1971**, 2034–2046.
(6) Bycroft, B. W. In *Chemistry and Biology of Peptides*; Meienhofer, J., Ed., Ann Arbor Science, Ann Arbor, MI 1972; pp 665–670.
(7) Hensens, O. D.; Albers-Schönberg, G.; Anderson, B. F. *J. Antibiot.* **1983**, *36*, 799–813.
(8) Noda, K.; Shimohigashi, Y.; Izumiya, N. In *The Peptides, Analysis, Synthesis, Biology*, Gross, E., Meienhofer, J., Eds., Academic: New York, 1983; Vol. 5, pp 285–339.
(9) English, M. L.; Stammer, C. H. *Biochem. Biophys. Res. Commun.* **1978**, *83*, 1464–1467.
(10) Ajo, D.; Granozzi, G.; Tondello, E.; Del Pra, A. *Biopolymers* **1980**, *19*, 469–475.
(11) Ajo, D.; Casarin, M.; Granozzi, G. *J. Mol. Struct.* **1982**, *86*, 297–300.
(12) Souhassou, M.; Lecomte, C.; Blessing, R. H.; Aubry, A.; Wiest, R.; Rohmer, M. M.; Benard, M. *Port. Phys. Proc. Sagamore IX Conf.* **1988**, *19*, 266–273.
(13) Aubry, A.; Allier, F.; Boussard, G.; Marraud, M. *Biopolymers* **1985**, *24*, 639–646.
(14) Blessing, R. H. *Crystallogr. Rev.* **1987**, *1*, 3–58.
(15) Blessing, R. H. *J. Appl. Crystallogr.* **1989**, *22*, 396–397.
(16) Allen, F. *Acta Crystallogr.* **1986**, *B42*, 515–522.
(17) Stewart, R. F.; Davidson, E. R.; Simpson, W. T. *J. Chem. Phys.* **1965**, *43*, 175–187.
(18) Clementi, E.; Raimondi, D. L. *J. Chem. Phys.* **1963**, 2686–2689.
(19) Cromer, D. T. In *International Tables for X-Ray Crystallography*; Ibers, J. A., Hamilton W. E., Ed.; Kynoch Press: Birmingham, England, pp 148–151.

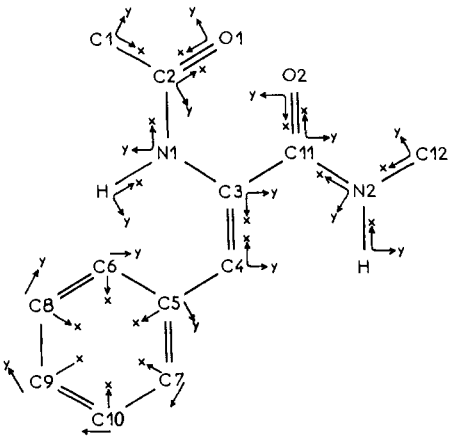

Figure 1. Directions of local Cartesian reference axes for the atom-centered multipole functions.

electron density maps by Fourier synthesis. This necessary accuracy can be attained using a multipolar atomic electron density model. Several multipolar refinements were done with different $(\sin\theta)/\lambda$ and $I/\sigma(I)$ cutoffs, and Hirshfeld,[20,21] Craven et al.,[22,23] and Hansen–Coppens[24] multipolar models were used. A comparison of the various models is given in detail in ref 25. All these refinements led to the same bonding density within 0.05 e Å^{-3}. The present paper describes the deformation density obtained with the Hansen–Coppens model (program Molly).[24] In this model, electron densities at each atom are described by

$$\rho(\mathbf{r}) = \rho_c(r) + P_v\kappa^3\rho_v(\kappa r) + \kappa'^3 \sum_{l=0}^{3} R_l(\kappa' r) \sum_{m=-l}^{+l} P_l^m y_l^m(\theta,\phi) \qquad (1)$$

where ρ_c and ρ_v are spherically averaged Hartree–Fock core and valence densities, y_l^m are the multipolar spherical harmonic angular functions in real form, and $R_l = N_l r^{n_l} e^{(-\kappa'\xi r)}$ are Slater-type radial functions, in which N_l is a normalization factor, and n_l and ξ are equal to values used in our previous work on *N*-acetyl-L-tryptophan methylamide.[3] The refinement variables are the valence shell contraction–expansion parameters κ and κ' and the population parameters P_v and P_l^m. The limit $l_{max} = 3$ corresponds to truncation of the expansion at the octopole level for the non-hydrogen atoms.[26] To reduce the number of variables, minimal symmetry constraints were imposed on the multipole parameters. Figure 1 gives the local coordinate systems. Local *mm2* symmetry was imposed on C_5 and on the chemically equivalent C_6–C_{10} atoms of the benzene ring, thus reducing the number of density parameters of the phenyl group from 108 to 16. No constraints were imposed on the atoms of the peptide units. Four types of hydrogen atoms were defined: H(sp^3) linked to the C_1 and C_{12} atoms, H(sp^2) linked to C_4 and to the benzene ring carbon atoms, H(N1) linked the nitrogen N_1 atom, and H(N2). For these hydrogen atoms the truncation of the spherical harmonic expansion was $l = 1$. With these assumptions, 219 density parameters and a total of 408 parameters were refined against the 6035 $[(I > 3\sigma(I)]$ unique reflections ($s < 1.35$ Å^{-1}). The P_v parameters are constrained in the Molly program in order that the total charge on the molecule is zero. Starting parameters were those of refinement I; the multipolar density parameters and the scale factor were initially refined with the structural parameters fixed at the refinement I values until convergence, and then all parameters were refined together (refinement V). As shown in Table I, the residual indices and the goodness of fit decreased dramatically when aspherical density was taken into account. The final residual densities of the benzene ring and of one peptide unit, calculated from refinement V and to a resolution of $s = 0.9$ Å^{-1} (calculation VI), are given in the supplementary material. All the valence density has been fitted, and the very low noise in these residual maps reflects the high quality of the data. For all refinements, the scale factor was extremely stable, the relative difference between the high-order refinements and multipolar refinement being $\Delta K/K = 0.6\%$. An isotropic extinction parameter was included in the refinement [$g = 3\ (1) \times 10^{-8}$ rad^{-1}]. Table II gives the fractional coordinates of all the atoms; Table III gives the anisotropic thermal motion parameters of the non-hydrogen atoms; the multipolar atomic electron density parameters are given in Table IV. The small populations of the quadrupole functions on the oxygen atoms might seem to be a surprising feature, but they are compensated by the sharpness of the radial dependence, which maximizes the oxygen lone pair densities close to the nuclear positions.

Table II. Fractional Coordinates of the Atoms and Standard Deviations

atom		*X*	*Y*	*Z*	*B*, Å^2
C_1	$C_{\alpha 0}$	−0.349 30 (5)	−0.341 70 (2)	−0.708 41 (6)	
C_2	C'_0	−0.356 48 (4)	−0.243 53 (2)	−0.740 16 (5)	
C_3	C_α	−0.218 30 (4)	−0.105 84 (2)	−0.650 60 (5)	
C_4	C_β	−0.112 37 (4)	−0.064 03 (2)	−0.672 93 (6)	
C_5	C_γ	−0.000 21 (5)	−0.105 64 (2)	−0.709 20 (6)	
C_6	$C_{\delta 1}$	−0.036 73 (5)	−0.178 17 (3)	−0.827 23 (7)	
C_7	$C_{\delta 2}$	0.148 18 (5)	−0.070 48 (3)	−0.625 20 (6)	
C_8	$C_{\epsilon 1}$	0.073 83 (6)	−0.215 79 (3)	−0.855 71 (7)	
C_9	$C_{\xi 1}$	0.222 58 (5)	−0.181 93 (3)	−0.766 63 (7)	
C_{10}	$C_{\epsilon 2}$	0.259 27 (5)	−0.108 83 (3)	−0.652 33 (7)	
C_{11}	C_1	−0.323 51 (4)	−0.055 86 (2)	−0.608 00 (5)	
C_{12}	$C_{\alpha 2}$	−0.474 04 (6)	0.077 40 (3)	−0.660 02 (7)	
O_1	O_0	−0.475 98	−0.206 06 (2)	−0.855 09	
O_2	O_1	−0.352 28 (4)	−0.085 52 (2)	−0.494 05 (5)	
N_1	N_1	−0.224 10 (4)	−0.198 86 (3)	−0.640 33 (5)	
N_2	N_2	−0.377 47 (4)	0.020 92 (2)	−0.695 42 (5)	
H101	$H_{\alpha 01}$	−0.4451	−0.3606	−0.6968	2.8 (2)
H201	$H_{\alpha 02}$	−0.2454	−0.3625	−0.5891	2.0 (2)
H301	$H_{\alpha 03}$	−0.3562	−0.3728	−0.8247	2.9 (2)
H104	H_β	−0.1062	0.0063	−0.6566	1.4 (1)
H106	$H_{\delta 1}$	−0.1512	−0.2036	−0.8990	1.7 (1)
H107	$H_{\delta 2}$	0.1739	−0.0154	−0.5354	1.9 (1)
H108	$H_{\epsilon 1}$	0.0454	−0.2716	−0.9443	2.1 (1)
H109	H_ξ	0.3082	−0.2126	−0.7852	2.6 (2)
H110	$H_{\epsilon 2}$	0.3734	−0.0829	−0.5818	3.0 (2)
H112	$H_{\alpha 21}$	−0.5833	0.0454	−0.7200	4.2 (2)
H212	$H_{\alpha 22}$	−0.4872	0.1376	−0.7324	4.9 (3)
H312	$H_{\alpha 23}$	−0.4244	0.0794	−0.5152	3.9 (2)
HO1	HN_1	−0.1272	−0.2313	−0.5424	1.1 (1)
HO2	HN_2	−0.3609	0.0382	−0.8003	1.2 (1)

(d) Electron Density Maps. In order to illustrate the asymmetry of the atomic charge distribution, experimental dynamic, and static, deformation maps were calculated. Experimental dynamic deformation maps are defined as

$$\delta_\rho^{exp}(\mathbf{r}) = \frac{1}{V}\sum_{\mathbf{H}} [(|F_o|/K)e^{i\phi_m(\mathbf{h})} - |F_s|e^{i\phi_s(\mathbf{h})}] \exp(-2\pi i\mathbf{h}\cdot\mathbf{r}) \qquad (2)$$

where the subscript m designates the atom-centered multipolar density model, and s the spherically averaged free atom superposition model. The scattering factor of the free, ground-state hydrogen atom was used to calculate the $|F_s|$ structure factors; $|F_o|/K$ is the scaled observed structure factor. The summation included the 3927 observed terms with $(\sin\theta)/\lambda < 1.00$ Å^{-1} and $I > 3\sigma(I)$ and refers to refinement V. The experimental maps defined by eq 2 thus include the effects of both finite experimental resolution and the convolution with the atomic thermal vibrations. Estimates of the average error in the experimental density maps are

$$\langle\sigma^2(\Delta\rho)\rangle^{1/2} = V^{-1}K^{-1}[\sum_{\mathbf{H}}\sigma^2(|F_o|)]^{1/2} = 0.029\ \bar{e}\ \text{Å}^{-3}$$

and

$$V^{-1}[\sum_{\mathbf{H}}(|F_o|K^{-1} - |F_m|)^2]^{1/2} = 0.032\ \bar{e}\ \text{Å}^{-3}$$

As shown in our previous paper,[3] the deformation density for a noncentrosymmetric crystal can be written as

$$\delta\rho(\mathbf{r}) = \delta\rho(\Delta|F|) + \delta\rho(\Delta\phi)$$

where

$$\delta\rho(\Delta|F|) = V^{-1}\sum_{\mathbf{H}}(|F_m| - |F_s|)\exp(i\phi_m)\exp(-2\pi i\mathbf{h}\cdot\mathbf{r}) \qquad (3)$$

and

$$\delta\rho(\Delta\phi) = V^{-1}\sum_{\mathbf{H}}[2|F_s|\sin(\Delta\phi/2)\exp i(\phi_s + \phi_m + \pi)/2]\exp(-2\pi i\mathbf{h}\cdot\mathbf{r})$$

Figure 2 shows the maps of the total deformation density $\delta\rho^{exp}(\mathbf{r})$, the

(20) Hirshfeld, F. L. *Acta Crystallogr.* **1971**, *B27*, 769–781.
(21) Hirshfeld, F. L. *Isr. J. Chem.* **1977**, *16*, 198–201.
(22) Craven, B. M.; Weber, H. P.; He, X. Technical Report TR-87-2, Department of Crystallography, U. of Pittsburgh, PA 15260, 1987.
(23) Epstein, J.; Ruble, J. R.; Craven, B. M. *Acta Crystallogr.* **1982**, *B38*, 140–149.
(24) Hansen, N.; Coppens, P. *Acta Crystallogr.* **1978**, *A34*, 909–921.
(25) Lecomte, C. In *The Application of Charge Density Research to Chemistry and Drug Design*; Geffrey, G. A., Ed. *NATO ASI Ser. B* **1991**, *No. 250*, 121–154.
(26) Hexadecapolar functions on the oxygen atoms did not significantly improve the statistics of the least squares fit.

Table III. Thermal Parameters of the Non-Hydrogen Atoms (Å² × 10⁵) and Estimated Standard Deviations[a]

atom		U^{11}	U^{22}	U^{33}	U^{12}	U^{13}	U^{23}
C_1	$C_{\alpha 0}$	1727 (12)	1105 (11)	1682 (12)	−65 (5)	385 (5)	−37 (5)
C_2	C'_0	941 (9)	1062 (10)	1065 (9)	−36 (4)	228 (4)	−21 (4)
C_3	C_α	876 (8)	1026 (10)	1105 (9)	−6 (4)	279 (4)	2 (4)
C_4	C_β	1078 (10)	1162 (11)	1616 (12)	−27 (4)	416 (5)	9 (5)
C_5	C_γ	1061 (10)	1428 (12)	1658 (11)	15 (4)	432 (4)	81 (5)
C_6	$C_{\delta 1}$	1721 (13)	1930 (15)	2224 (15)	−63 (6)	723 (6)	−192 (6)
C_7	$C_{\delta 2}$	1114 (11)	2104 (15)	2017 (14)	−76 (5)	446 (5)	117 (6)
C_8	$C_{\epsilon 1}$	2420 (16)	2479 (18)	2670 (17)	191 (7)	977 (8)	−33 (7)
C_9	C_ξ	1811 (14)	3457 (21)	2430 (17)	455 (7)	784 (7)	331 (8)
C_{10}	$C_{\epsilon 2}$	1132 (12)	3517 (21)	2254 (16)	101 (6)	513 (6)	278 (7)
C_{11}	C'_1	1083 (9)	1085 (10)	1017 (9)	35 (4)	325 (4)	23 (4)
C_{12}	$C_{\alpha 2}$	2466 (15)	1823 (15)	2018 (14)	481 (6)	778 (6)	218 (6)
O_1	O_0	934 (7)	1417 (9)	1464 (9)	−47 (4)	84 (4)	24 (4)
O_2	O_1	1892 (10)	1368 (9)	1450 (9)	44 (4)	621 (4)	69 (4)
N_1	N_1	795 (7)	974 (9)	1180 (8)	3 (4)	199 (3)	14 (4)
N_2	N_2	1659 (10)	1279 (10)	1355 (10)	217 (4)	515 (4)	147 (4)

[a] $f(T) = f(0) \exp[-2\pi^2 \sum_{j=1}^{3}\sum_{k=1}^{3} h_j h_k a^{*j} a^{*k} U^{jk}]$.

Table IV. Multipolar Atomic Electron Density Parameters[a]

atom		P_v	P_1^1	P_1^{-1}	P_1^0	P_2^0	P_2^1	P_2^{-1}	P_2^2	P_2^{-2}	P_3^0	P_3^1	P_3^{-1}	P_3^2	P_3^{-2}	P_3^3	P_3^{-3}	κ	$\kappa'\xi$, bohr^{-1}
C_1	$C_{\alpha 0}$	4.25 (4)	−0.05	0.05	0.01	0.05	0.01	−0.00	−0.07	−0.04	0.03	−0.26	−0.19	0.02	−0.02	0.23	0.08	0.99	2.66
C_2	C'_0	3.87 (3)	0.13	0.05	−0.04	−0.32	−0.01	0.02	0.11	−0.03	0.01	−0.05	−0.01	0.00	−0.01	0.40	0.00	1.02	2.69
C_3	C_α	4.10 (4)	0.16	0.09	−0.06	−0.17	−0.01	−0.03	0.10	−0.04	0.01	0.06	0.05	0.03	0.02	0.32	0.03	1.00	2.81
C_4	C_β	3.88 (4)	0.02	0.04	0.05	−0.19	0.00	0.02	0.01	0.01	0.01	0.07	0.03	0.01	−0.04	0.32	0.02	1.02	2.76
C_5	C_γ	4.02 (3)	−0.02			−0.24			−0.04			0.05				−0.33		1.00	2.70
C_6[b]	C_δ	4.10 (1)	0.03			−0.23			−0.01			0.01				−0.33		1.00	2.86
C_{11}	C'_1	4.10 (3)	0.08	−0.04	−0.01	−0.31	−0.02	−0.01	0.10	−0.01	0.00	−0.01	0.01	0.02	−0.03	0.43	0.05	1.00	2.76
C_{12}	$C_{\alpha 2}$	4.32 (4)	−0.15	−0.11	0.02	0.06	0.04	0.04	−0.02	0.01	0.01	−0.35	0.05	−0.08	−0.04	0.36	−0.07	0.97	2.52
N_1	N_1	5.31 (3)	0.05	0.05	−0.02	−0.02	0.01	−0.00	0.01	−0.03	0.01	0.03	0.02	0.01	0.03	0.26	0.03	0.99	3.40
N_2	N_2	5.08 (3)	0.01	0.09	−0.03	−0.00	0.02	−0.04	−0.02	−0.02	0.02	0.00	0.01	0.01	−0.02	0.21	0.00	1.00	3.26
O_1	O_0	6.37 (2)	−0.09	0.03	0.04	−0.04	0.00	−0.01	−0.04	−0.00	0.02	0.02	0.01	−0.02	−0.02	0.04	0.00	0.97	4.04
O_2	O_1	6.45 (2)	−0.07	0.03	0.00	−0.06	0.01	−0.02	−0.04	0.02	0.00	−0.00	0.01	−0.01	−0.02	0.01	−0.00	0.98	4.50
HC(sp3)		0.87 (1)	0.17 (1)															1.11[c]	2.26
HC(sp2)		0.84 (1)	0.14 (1)															1.09[c]	2.26
HN_1		0.75 (2)	0.15 (1)															1.15[c]	2.26
HN_2		0.76 (2)	0.18 (2)															1.10[c]	2.26

[a] See Figure 1 for the directions of local orthonormal reference axes and eq 1 for explanation of the κ, κ', and P_l^m parameters: $n_l = 2, 2, 3$, respectively, for $l = 1, 2$, and 3 for the C, O, N atoms and $n_l = 1$ for the hydrogen dipole functions. For the P_l^m and κ, κ' values, the average standard deviation is 0.01. [b] $C_\delta \equiv C_\epsilon \equiv C_\xi$. [c] Relative to the free ground-state hydrogen form factor.

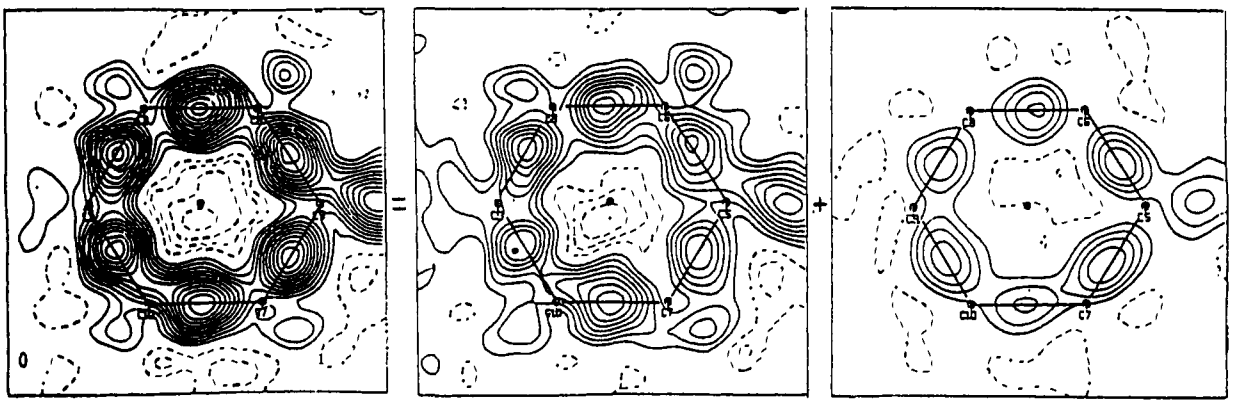

Figure 2. Maps of the total experimental $\delta\rho^{exp}(r)$ (a), of $\delta\rho|\Delta F|$ (b), and $\delta\rho(\Delta\phi)$ (c) in the plane of the benzene ring. Contour interval 0.05 e Å^{-3}; positive contours solid, negative contours dashed; zero contour omitted.

magnitude contribution $\delta\rho|\Delta F|$, and the phase contribution $\delta\rho(\Delta\phi)$ for the benzene ring. The $\delta\rho|\Delta F|$ map was calculated with $|F_m|$ in eq 3 replaced by $K^{-1}|F_o|$. As shown in Figure 2, the maximum and average of $\Delta\rho(\Delta\phi)$ are 0.23 and 0.19 e Å^{-3}, respectively. Furthermore, the addition of $\Delta\rho(\Delta\phi)$ clearly contributes to make the C–C bonding densities equivalent.

Quantum Chemical Calculations. Ab initio SCF calculations were carried out on (*Z*)-*N*-acetyl-α,β-dehydrophenylalanine methylamide using the crystallographic molecular geometry and the IBM version of the ASTERIX program system (for a CRAY version of this program, see refs 27–30). Two basis sets were used, as described in Table V. Basis sets I are medium-size, split-valence basis sets taken from Huzinaga,[31] in which first row atoms are described with 9s and 5p Gaussian-type orbitals (GTOs) contracted into [3s, 2p]. Hydrogen is described with 4s-type GTOs contracted into 2. In basis set II, more flexibility has been allowed to the description of the atomic valence shells by adopting a

(27) Ernenwein, R.; Rohmer, M. M.; Bénard, M. *Comput. Phys. Commun.* **1990**, *58*, 305.
(28) Rohmer, M. M.; Demuynck, J.; Bénard, M.; Wiest, R.; Bachmann, C.; Henriet, C.; Ernenwein, R. *Comput. Phys. Commun.* **1990**, *60*, 127.
(29) Wiest, R.; Demuynck, J.; Bénard, M.; Rohmer, M. M. *Comput. Phys. Commun.* **1991**, *62*, 107.
(30) Rohmer, M. M.; Ernenwein, R.; Ulmschneider, M.; Wiest, R.; Bénard, M. *Int. J. Quantum Chem.* **1991**, *40*, 723–744.
(31) Huzinaga, S. *Technical Report, University of Alberta, Edmonton, Canada*, **1971**.

Table V. Exponents and Contraction Scheme for Gaussian Basis Sets I and II

CGTO type	CGTO no.	exponents							
		C_I	C_{II}	N_I	N_{II}	O_I	O_{II}	H_I	H_{II}
s	1	0.42403098 + 4	0.42403098 + 4	0.60242736 + 4	0.60242736 + 4	0.804616 + 4	0.804616 + 4	0.133615 + 2	0.681600 + 2
		0.63777827 + 3	0.63777827 + 3	0.90659577 + 3	0.90659577 + 3	0.121198 + 4	0.121198 + 4	0.201330 + 1	0.102465 + 2
		0.14674534 + 3	0.14674534 + 3	0.20844780 + 3	0.20844780 + 3	0.279525 + 3	0.279525 + 3	0.453757 + 0	0.234648 + 1
		0.42531428 + 2	0.42531428 + 2	0.60103683 + 2	0.60103683 + 2	0.809330 + 2	0.809330 + 2		0.673320 + 0
		0.14184804 + 2	0.14184804 + 2	0.19973348 + 2	0.19973348 + 2	0.269343 + 2	0.269343 + 2		
		0.51756943 + 1	0.51756943 + 1	0.73341985 + 1	0.73341985 + 1	0.983933 + 1	0.983933 + 1		
		0.20072531 + 1	0.20072531 + 1	0.28938194 + 1	0.28938194 + 1	0.383404 + 1	0.383404 + 1		
	2	0.49677422 + 0	0.49677422 + 0	0.70806350 + 0	0.70806350 + 0	0.956811 + 0	0.956811 + 0	0.123317 + 0	0.224660 + 0
	3	0.15348718 + 0	0.15348718 + 0	0.21581223 + 0	0.21581223 + 0	0.288996 + 0	0.288996 + 0		0.822170 − 1
	4		0.50 − 01		0.70 − 01		0.90 − 01		
p	1	0.18099144 + 2	0.18099144 + 2	0.26362609 + 2	0.26362609 + 2	0.349066 + 2	0.349066 + 2		0.80 + 00
		0.39769145 + 1	0.39769145 + 1	0.58777343 + 1	0.58777343 + 1	0.784656 + 1	0.784656 + 1		
		0.11450768 + 1	0.11450768 + 1	0.17167892 + 1	0.17167892 + 1	0.230499 + 1	0.230499 + 1		
		0.36188831 + 0		0.54594357 + 0		0.722057 + 0			
	2	0.11460548 + 0	0.36188831 + 0	0.16994634 + 0	0.54594357 + 0	0.215259 + 0	0.722057 + 0		
	3		0.11460548 + 0		0.16994634 + 0		0.215259 + 0		
d	1		0.630 + 00		0.950 + 00		0.133 + 01		

triple-ζ contraction completed with one p-type (for hydrogen) or one d-type (for C, N, and O) polarization function. For hydrogen, basis set II is therefore a (6,1) basis set contracted into [3, 1]. It is taken from Huzinaga,[32] and its exponents are not related to those of basis set I (Table V). At variance from that, the same exponents used for the split-valence basis sets of C, N, and O have been kept in the large basis sets. The most apparent drawbacks of basis sets I, as far as deformation density is concerned, have been corrected in the following way:

(1) A more diffuse function (exponents 0.09 for O, 0.07 for N, and 0.05 for C) has been added to the s shell according to the even-tempered criterion. The density maximum associated with this diffuse function is close to that of the outermost p function.

(2) The penultimate p-type function (exponents 0.722 057 for O, 0.545 944 for N, and 0.361 888 for C) whose density maximum varies from 0.6 to 0.9 Å has an obviously important participation in the deformation density buildup. Keeping this GTO contracted together with three p-type functions having higher exponents could appreciably restrain the orbital flexibility. It has therefore been left uncontracted in basis set II (Table V).

(3) The importance of polarization functions for generating accurate deformation density maps is well documented.[33-37] Exponents used for the 3d functions (1.33 for O, 0.95 for N, and 0.63 for C) are taken from the work of Roos and Siegbahn.[38] Eventually, basis sets II for C, N, and O are (10, 5, 1) contracted into [4, 3, 1]. It should be noticed that the quality of basis set II appears very close to that used by Stevens, Rys, and Coppens[39] for the benchmark calculations on the electron distribution density of formamide.

Two ab inito SCF calculations were carried out. In the first calculation, all atoms were described with basis set I, thus yielding a molecular basis set containing 440 GTOs, contracted into 172. In the second calculation, basis set II was used for all atoms but those belonging to the two methyl and to the phenyl substituents, for which basis sets I were retained. The molecular basis set in this calculation contained 511 GTOs contracted into 264. In relation to the absence of molecular symmetry, the number of supermatrix elements to be computed, stored, and iteratively processed in the second calculation was as high as 356 836 987.

Results

Molecular Conformation. Figure 3 shows the molecular structure, and selected valence and conformation angles are given in Table VI; the bond distances are given with the peaks heights in Table IX. The molecular conformation did not change from room temperature to 100 K (Table VI) and the present study fully confirms the conclusions drawn by Aubry et al.[13]: The existence of the C_α=C_β double bond leads to a phenyl orientation that is forbidden in phenylalanine [χ_1 = 6.97 (6)°] and to shorter C_α–C_β and C_β–C_γ distances [1.3473 (7) and 1.4717 (7) Å]. The C_α atom

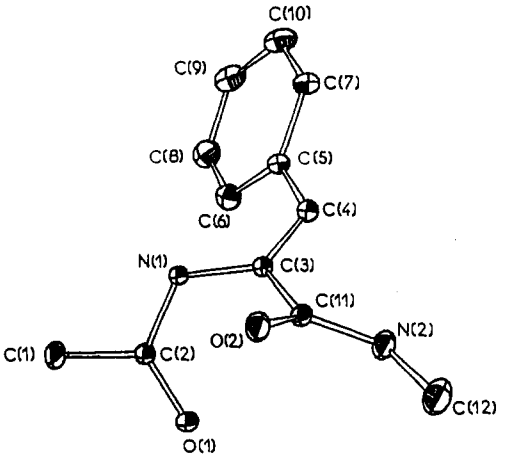

Figure 3. ORTEP drawing of the molecule. The thermal ellipsoids are shown at 50% probability.

Table VI. Selected Valence and Conformation Angles (deg)

C_1–C_2–O_1	$C_{\alpha 0}$–C'_0–O_0	122.07 (3)
C_1–C_2–N_1	$C_{\alpha 0}$–C'_0–N_1	116.16 (3)
O_1–C_2–N_1	O_0–C'_0–N_1	121.74 (3)
C_2–N_1–C_3	C'_0–N_1–C_α	121.34 (3)
N_1–C_3–C_4	N_1–C_α–C_β	122.57 (4)
N_1–C_3–C_{11}	N_1–C_α–C'_1	115.30 (4)
C_{11}–C_3–C_4	C'_1–C_α–C_β	121.57 (3)
C_3–C_{11}–N_2	C_α–C'_1–N_2	116.08 (5)
C_3–C_{11}–O_2	C_α–C'_1–O_1	119.89 (3)
O_2–C_{11}–N_2	O_1–C'_1–N_2	124.00 (5)
C_{11}–N_2–C_{12}	C'_1–N_2–$C_{\alpha 2}$	121.50 (5)
C_3–C_4–C_5	C_α–C_β–C_γ	126.62 (3)
C_4–C_5–C_6	C_β–C_γ–$C_{\delta 1}$	122.65 (4)
C_6–C_5–C_7	$C_{\delta 1}$–C_γ–$C_{\delta 2}$	118.66 (5)
C_4–C_5–C_7	C_β–C_γ–$C_{\delta 2}$	118.68 (4)
C_5–C_7–C_{10}	C_γ–$C_{\delta 2}$–$C_{\epsilon 2}$	120.74 (4)
C_7–C_{10}–C_9	$C_{\epsilon 2}$–$C_{\xi 1}$–$C_{\epsilon 1}$	120.04 (4)
C_{10}–C_9–C_8	C_ξ–$C_{\epsilon 1}$–$C_{\delta 1}$	119.75 (6)
C_9–C_8–C_6	$C_{\epsilon 1}$–$C_{\delta 1}$–C_γ	120.26 (5)
C_8–C_6–C_5		120.50 (4)

	a	*b*
$\omega_1 = C_{\alpha 0}$–C'_0–N_1–C_α = C_1–C_2–N_1–C_3 =	−176.39 (5)	−177.2
$\omega_2 = C_\alpha$–C'_1–N_2–$C_{\alpha 2}$ = C_3–C_{11}–N_2–C_{12} =	−177.04 (3)	−175.4
$\phi = C'_0$–N_1–C_α–C'_1 = C_2–N_1–C_3–C_{11} =	56.81 (6)	58.3
$\psi = N_1$–C_α–C'_1–N_2 = N_1–C_3–C_{11}–N_2 =	−148.71 (3)	−148.0
$\chi_1 = N_1$–C_α–C_β–C_γ = N_1–C_3–C_4–C_5 =	6.97 (6)	7.8
C_{11}–C_3–C_4–C_5 =	177.98 (3)	
$\chi_{2,1} = C_\alpha$–C_β–C_γ–$C_{\delta 1}$ = C_3–C_4–C_5–C_6 =	39.76 (6)	37.5
$\chi_{2,2} = C_\alpha$–C_β–C_γ–$C_{\delta 2}$ = C_3–C_4–C_5–C_7 =	−141.44 (4)	−143.3
C_2–N_1–C_3–C_4 =	−131.66 (5)	
C_4–C_3–C_{11}–N_2 =	39.66 (5)	

[a] This work. [b] Room temperature structure from ref 13.

is 0.06 Å above the N1, C'_1, C_β, C_γ plane. Furthermore the C'_0–N_1 bond [1.3470 (4) Å] appears to be slightly longer than

(32) Huzinaga, S. *J. Chem. Phys.* **1965**, *42*, 1293.
(33) Bader, R. F. W. *MTP Int. Rev. Sci.: Phys. Chem., Ser. 2* **1975**, *1*, 43.
(34) Cade, P. E. *Trans. Am. Crystallogr. Assoc.* **1972**, *8*, 1–36.
(35) Heijser, W.; Baerends, E. J.; Ros, P. *J. Mol. Struct.* **1980**, *63*, 109.
(36) Hall, M. B. In *Electron Distributions and the Chemical Bond*; Coppens, P.; Hall, M. B., Eds.; Plenum Press: New York, 1982; pp 205–220.
(37) Kunze, K. L.; Hall, M. B. *J. Am. Chem. Soc.* **1986**, *108*, 5122.
(38) Roos, B.; Siegbahn, P. *Theor. Chim. Acta* **1971**, *17*, 199.
(39) Stevens, E. D.; Rys, J.; Coppens, P. *J. Am. Chem. Soc.* **1978**, *100*, 2324.

Chart II

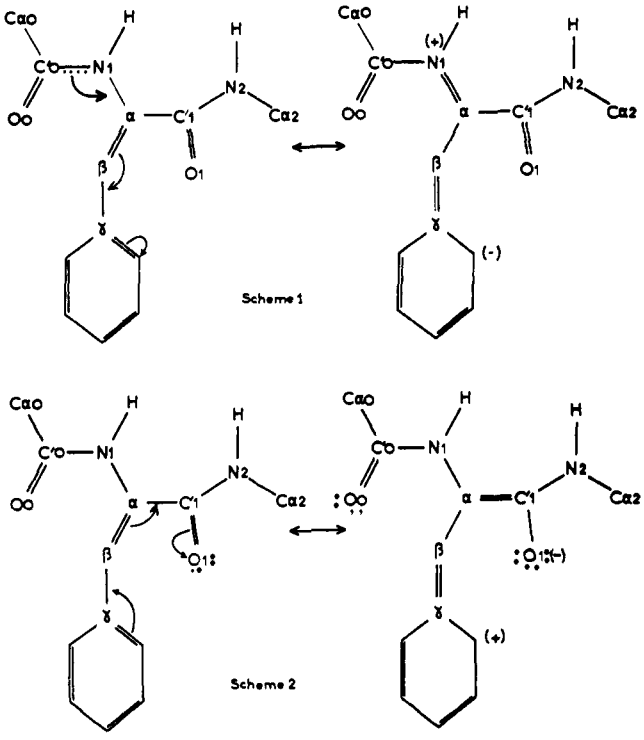

the corresponding C'_1–N_2 bond [1.3356 (4) Å] whereas C_α–N_1 [1.4118 (4) Å] is shorter than $C_{\alpha 2}$–N_2 [1.448 (8) Å]. Finally, the C_α–C'_1 bond [1.5027 (7) Å] is 0.04 Å shorter than the corresponding bond in *N*-acetyl-L-tryptophan methylamide[3] [1.541 (1) Å]. These bond length differences can be explained by two electron conjugation schemes (Chart II), although the ideal case for electron conjugation would imply the planarity of C_2–N_1–C_3–C_4 (Scheme 1) or C_4–C_3–$C_{11}N_2$ (Scheme 2), which is not exactly the case (Table VI). If scheme 2 is favored, we would expect a higher net charge on the C'_1O_1 group, whereas Scheme 1 would lead to a more positive N_1 atom. However, the electronic effects must be very small, according to the small bond length differences. Finally, the C_γ–C_δ bond lengths of the phenyl ring [1.403 (1) Å] and the corresponding C_δ–C_γ–C_δ bond angle [118.66 (5)°] are different from the other carbon–carbon bond distances and angles of the phenyl ring [⟨C–C⟩ = 1.394 (1) Å, ⟨C–C–C⟩ = 120.25 (5)°] in agreement with electron conjugation of the C_α=C_β double bond with the phenyl ring. As observed by Aubry et al.[13] (Figure 3 of ref 13), the molecules associate in rows by means of two single hydrogen bonds (⟨N···O⟩ = 2.85 Å).

Thermal Vibration Analysis. The Hirshfeld rigid bond test[40] indicated that the high-order refinement and the multipole refinement yielded an effective deconvolution of the mean-square atomic displacements from the valence electron density deformations. The differences between mean-square atomic displacements along bond directions had magnitudes $|\Delta| \leq 0.0008$ Å^2 for all the bonded pairs of non-hydrogen atoms. Along nonbonded intramolecular interatomic directions some $|\Delta|$ values were considerably larger, indicating that the molecule is not entirely rigid and that low-frequency, soft modes of internal vibration contribute significantly to the observed mean-square displacements. These modes were modeled by fitting molecular T, L, and S plus correlated ϕ_i tensors to the atomic *U* tensors: The T, L, and S model the external lattice vibrations of the whole molecule; the ϕ_i model low-frequency, large-amplitude internal molecular vibrations as librations of rigid groups of atoms within the flexible molecule.[41-43] Various models for the internal vibrations were tried. The best results (R = 3.5%) are summarized in Table VII. The most important librations are with C_α as a flexible joint linking three librating rigid groups. This model is in complete agreement with our results on *N*-acetyl-L-tryptophan methylamide,[3] which also shows that the softer librations correspond to the ϕ_1 and ψ_1 torsion angles (Table VII).

Table VII. Statistics of Fit, Principal Mean-Square Amplitudes, and Torsional Force Constants from the Fit of Molecular TLS[a] + Φ_l to the Atomic U^{jk}

	rigid molecule	flexible molecule	whole molecule: translations ⟨t^2⟩, Å^2	whole molecule: librations ⟨λ^2⟩, deg^2
R = $(\chi^2/\sum wU^{jk2})^{1/2}$ [b]	15%	3.5%	0.0133	4.68
S = $[\chi^2/(m-n)]^{1/2}$ [b]	7.00	2.22	0.0110	3.17
n "observs" U^{jk}	96	96	0.0079	1.64
m parameters	20	44		

librating group	libration axis	torsion angle	⟨ϕ^2⟩, deg^2	force const, J mol^{-1} deg^{-2}
$C_{\alpha 0}$–C_0–O_0 about	C_α–N_1	ϕ_1	18.7 (1.8)	47.5 (5)
$C_{\alpha 2}$–N_2–O_1 about	C_α–C_1	ψ_1	11.4 (2.4)	89.8 (18)
phenyl ring about	C_α–C_β	χ_1	4.2 (1.8)	214.9 (68)
phenyl ring about	(C_3, C_4, C_5) trough C_4	valence angle bending	2.0 (0.6)	466.8 (110)

T[c]	=	0.00801 (24)	0.00047 (18)	−0.00045 (32)
			0.01091 (25)	0.00031 (24)
				0.01323 (53)
L[d]	=	0.00107 (17)	0.00038 (26)	−0.00010 (7)
			0.00077 (23)	−0.00018 (22)
				−0.00104 (8)
S[e]	=	0.00077 (15)	0.00016 (16)	−0.00036 (25)
		0.00012 (32)	−0.00036 (18)	−0.00207 (40)
		0.00019 (11)	0.00102 (11)	−0.00040 (19)

[a] T, L, and S tensors refer to Cartesian axes with x along a, z along c^*. [b] $\chi^2 = \sum w[U^{jk} - U^{jk}(\mathrm{TLS} + \phi_l)]^2$ where $w = 1/\sigma^2(U^{jk})$. [c] In Å^2. [d] In radian^2. [e] In Å × radian.

Table VIII. Experimental Net Charges (ē) of Atoms and Groups of the Molecule

$C_{\alpha 0}H_3$	0.15	$C_{\alpha 2}H_3$	0.07	C_α	−0.10
C'_0	0.13	C'_1	−0.10	$C_\beta H$	0.28
N_1H	−0.06	N_2H	0.15	C_γ	−0.02
O_0	−0.37	O_1	−0.44	$C_\delta H$	0.06
N terminal link	−0.15	C terminal link	−0.32	side chain	0.56
				C_α included	0.46

Net Charges from Multipole Refinement. Table VIII gives the net charges of the atoms or groups calculated from the multipole refinement. The total charge of both peptide units ($C_\alpha C'ONH$) is negative, respectively, −0.15 ē for the N terminal unit and −0.32 ē for the C terminal unit, in agreement with conjugation scheme 2, which favors more negative charge on the C'_1O_1 group (−0.54 ē) than on the C'_0O_0 group (−0.24 ē). Furthermore, the N_1 atom is more negatively charged (N_1 = −0.30 ē versus −0.08 for N_2) in disagreement with Scheme 1.

Experimental Deformation Maps. Figure 4 gives the experimental deformation density maps of the C terminal peptide unit (a) and of the N terminal peptide unit (b). The very low noise confirms the quality of the experimental data. As observed before for *N*-acetyl-L-tryptophan methylamide,[3] the C–N peak heights are related to the bond length and π character. Very little difference between the two peptide units appears on the maps. Bonding maxima of equivalent bonds are equal within 0.05 ē Å^{-3} and the only barely significant differences are the following: The C'_0···N_1 bond peak is not centered on the C'_0–N_1 bond as observed for C'_1–N_2 and for all C–N bonds of *N*-acetyl-L-tryptophan methylamide, leading to a higher integrated net charge on the

(40) Hirshfeld, F. L. *Acta Crystallogr.* **1976**, *A32*, 239–244.
(41) Rosenfeld, R. E., Jr.; Trueblood, K. N.; Dunitz, J. D. *Acta Crystallogr.* **1978**, *A34*, 828.
(42) Dunitz, J. D.; Shomaker, V.; Trueblood, K. N. *J. Phys. Chem.* **1988**, *92*, 856–867.
(43) Dunitz, J. D.; Maverik, E. F.; Trueblood K. N. *Angew. Chem., Int. Ed. Engl.* **1988**, *27*, 880–895.

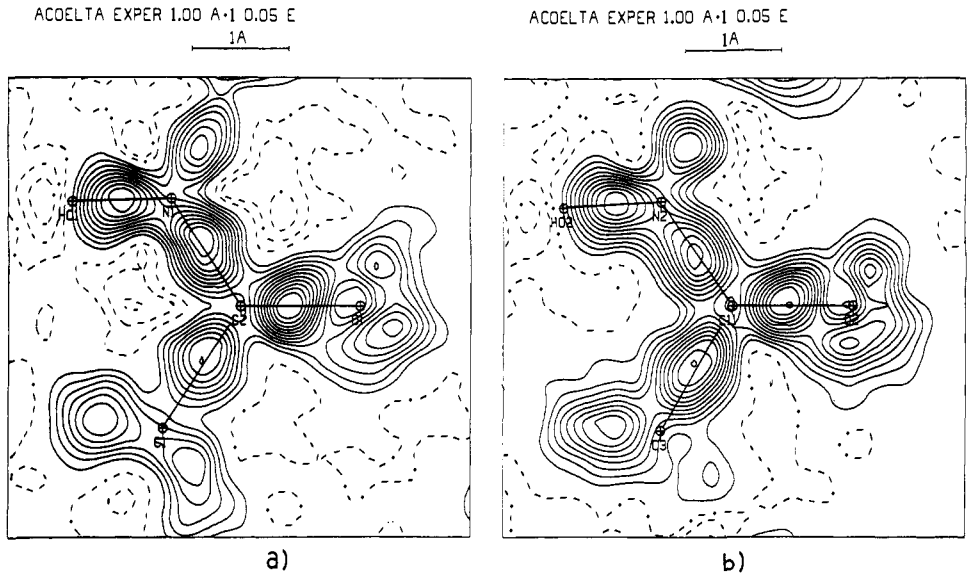

Figure 4. Experimental dynamic deformation density in the plane of the C terminal peptide group (a) and of the N terminal peptide group (b). Contours as in Figure 2.

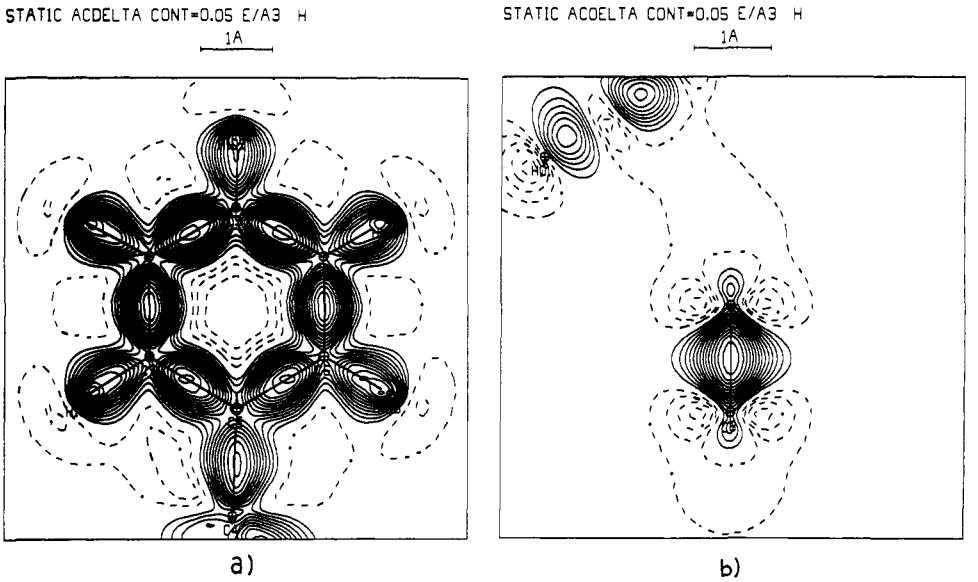

Figure 5. Crystallographic static deformation density in the plane of the benzene ring (a) and in a plane perpendicular to the benzene ring passing through a C–C bond (b). Contours as in Figure 2.

N_1 atom in disagreement with conjugation Scheme 1; also the C=O deformation density of the C terminal bond is slightly higher, in agreement with our conclusions based on the net charges. However, these small effects, which are in accordance with the short C_α–C'_1 distance, are not visible in the theoretical deformation density maps (see below) and must therefore be interpreted with care.

The crystallographic static deformation density maps in the plane of the benzene ring and in a plane perpendicular to the phenyl ring passing through one C–C bond are shown Figure 5; the π character of the bond is clearly revealed by the depletion of the p_z density of the carbon atoms and by the elliptic shape and the height (0.72 e Å^{-3}) of the bonding density. For comparison, Figure 6 shows the static deformation densities of the π plane of the C_α—C′ bond (a) and of the C_α=C_β double bond (b). The peaks heights and the shapes are in excellent agreement with the increasing π character of the bonds. The p_z depletion visible on the C'_1 atom must be related to the π character of the C′–N and C′–O peptide bonds (Figure 7a,b). The π-nonbonding density of the N atom clearly appears on the static deformation density maps (Figure 7a). These densities were not so apparent on the dynamic experimental deformations maps of *N*-acetyl-L-tryptophan methylamide,[3] because of the finite resolution of, and thermal motion convolution with, the deformation density.

Hydrogen Bonds. Each oxygen atom accepts one intermolecular hydrogen bond [$N_1\cdots O_1$ = 2.8349 (5) Å, $N_2\cdots O_2$ = 2.8694 (9) Å]. Figure 8 shows the experimental static deformation density in the plane defined by the HO_1, O_1, C_1 atoms; the N_1 nitrogen atom lies –0.12 Å out of the plane; the N_1–H bond is directed exactly toward one of the O_1 oxygen lone pairs. Furthermore, an important –0.25 ē Å^{-3} density minimum occurs close to the HN_1 atom, between it and O_1. A similar minimum (–0.20 ē Å^{-3}) occurs close to the HN_2 atom for the $N_2\cdots O_2$ hydrogen bond although the lone pair of O_2 is not exactly directed toward HO_2 (Figure 8b). These significant minima do not appear for the other hydrogen atoms not involved in hydrogen bonds (see Figure 5a for example) and are consistent with an electrostatic description of hydrogen bonding.

Basis Set Quality. Deformation density maps obtained from ab initio SCF calculations with basis sets I and II are displayed in three planes defined by the following atomic triads: (i) C_3–C_4–N_1 (Figure 9), (ii) C_3–C_{11}–O_2 (Figure 10), (iii) N_1–C_2–O_1 (Figure 11). The difference

$$\rho_{mol}(\text{basis II}) - \rho_{mol}(\text{basis I})$$

is also displayed. It should be noted first that the shape and height

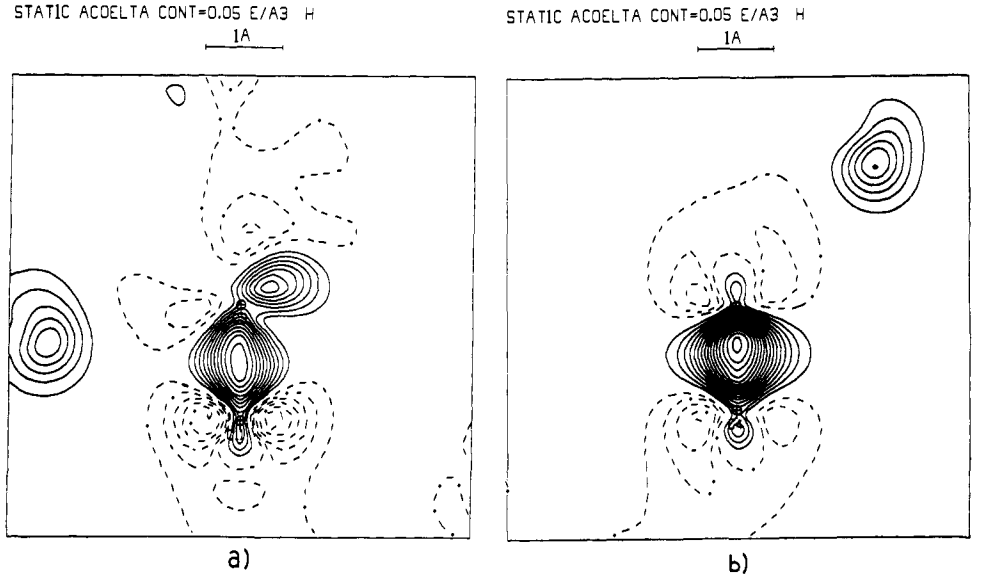

Figure 6. Crystallographic static deformation densities in the π planes of the C_α—C′ (a) and C_α=C_β (b) bonds. Contours as in Figure 2.

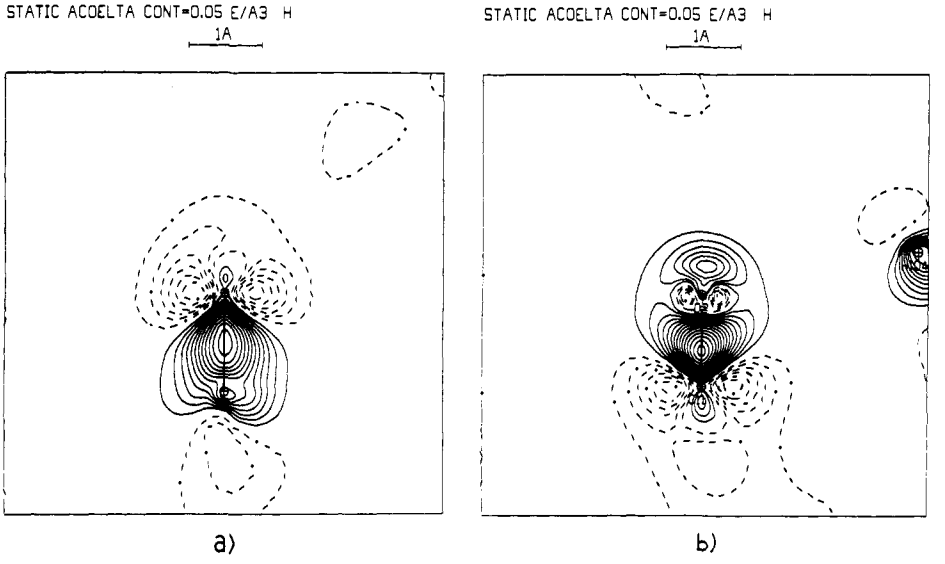

Figure 7. Crystallographic static deformation density in the π planes of the C′–N (a) and C′=O (b) bonds. Contours as in Figure 2.

of the density peaks obtained with basis set II along the C—N, C=O, and N—H bonds are quite similar to those obtained in the static theoretical density calculated in the study on formamide (see Figure 2 of ref 39). The depletion regions centered along the C—O axes at ~0.25 Å from the oxygen nuclei are also quite similar in both calculations, as are the lone pair accumulations. Around the nitrogen atoms, depopulation regions with three minima opposite to the bond axes (–0.3 to –0.4 e Å^{-3}) are obtained in both calculations. Such a quantitative similarity between the calculated maps of formamide and both peptide groups of *N*-AcΔPhe–NHMe shows that the charge density of a localized bond is at the present level of accuracy a local and quite transferable property. One can thus conclude that the density pattern of equivalent functional groups is transferable without substantial modifications *from one isolated molecule to a different isolated molecule.*

The effect of basis set extension is clearly visible in the difference maps ρ_{mol}(basis II)–ρ_{mol}(basis I) (Figures 9c, 10c, and 11c). The height of the bond peaks is consistently increased by 0.18 e Å^{-3} for the C_3=C_4 double bond, by 0.21 e Å^{-3} for the C_3—C_{11} bond, and by 0.23–0.27 e Å^{-3} for the C–N bonds. For the C=O bonds, in which the distribution of the residual density is most asymmetric, the peak height obtained with basis set II is increased by 0.24 e Å^{-3}, but the maximum difference between basis sets I and II exceeds 0.4 e Å^{-3}. The largest increase is obtained at 0.53 Å from the oxygen nucleus, that is, near the point of zero residual density (Figure 11). Extending the basis set reduces the depopulation region, increases the peak height, and displaces the peak by 0.16 Å toward oxygen. The displacement of the peak is negligible for the other bonds. In contrast with the increase of deformation density along the bonds, the regions opposite to the bond axes are more depleted with basis set II than with basis set I. The accumulations associated with the oxygen lone pairs are also reduced by 0.25 e Å^{-3}.

In general, the extension of the basis set quantitatively accentuates the contrast between buildup and depletion regions that had been outlined with reasonable geometrical precision using basis set I. It is interesting to notice in that respect that the very sensitive zero contour is scarcely affected by the basis set extension.

Agreement between Theory and Experiment

Figure 12 gives the crystallographic static deformation density maps of the two peptide links (a, b) calculated in the same planes as the theoretical maps. The C_α=C_β double bond is shown Figure 13. As observed on the experimental maps, the static maps do not reveal a real significant difference between the two peptide bonds due to the α–β dehydrogenation. These thermal-motion-deconvoluted experimental maps should compare best with the theoretical ones (Figures 9–11). Basis set I provides a fair qualitative agreement with experiment concerning the positions

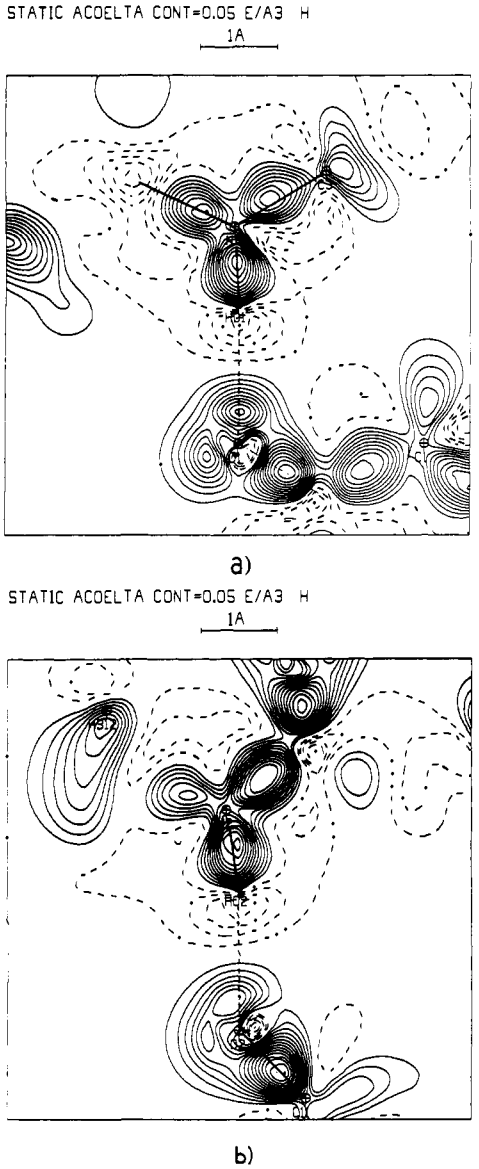

Figure 8. Static deformation density in the planes of the hydrogen bonds N_1–H_1···O_1 (a) and N_2–H···O_2 (b). Contours as in Figure 2.

of the maxima and the minima of the deformation density. As expected, however, the theoretical peak heights are systematically underestimated, the quantitative discrepancy being particularly large along the C—N and C=O bonds. A similar but smaller discrepancy is also visible in our work on *N*-acetyl-L-tryptophan methylamide.[1-3] The quantitative improvement is impressive with basis set II. Table IX provides a comparison of the peak heights obtained from experimental, static model and theoretical deformation density distributions. All bond peak heights obtained from the static model and theoretical distributions are equal within three experimental estimated standard deviations (3σ = 0.1 e Å^{-3}) except for the C_4–H_4 peak for which the difference reaches 0.21 e Å^{-3}. A much better agreement was obtained for the N–H bond peaks. In fact, such a small difference in the C–H bonds is very satisfactory and shows that the hydrogen modeling in the experimental analysis is realistic even though no neutron data are available.

Quantitative discrepancies remain important in the region of the oxygen lone pairs, since the peaks obtained on the static maps are 0.50–0.60 e Å^{-3} compared to more than 1 e Å^{-3} in the theoretical maps. A part of the discrepancy can be attributed to the fact that theory calculates the deformation density of the molecule in vacuo, whereas the experiment shows a pseudoisolated, pseudostatic molecule removed from the crystal lattice; the lone pairs can then be different because of the intermolecular hydrogen bonds. Similar patterns were reported for β-DL-arabinose:[44] Both

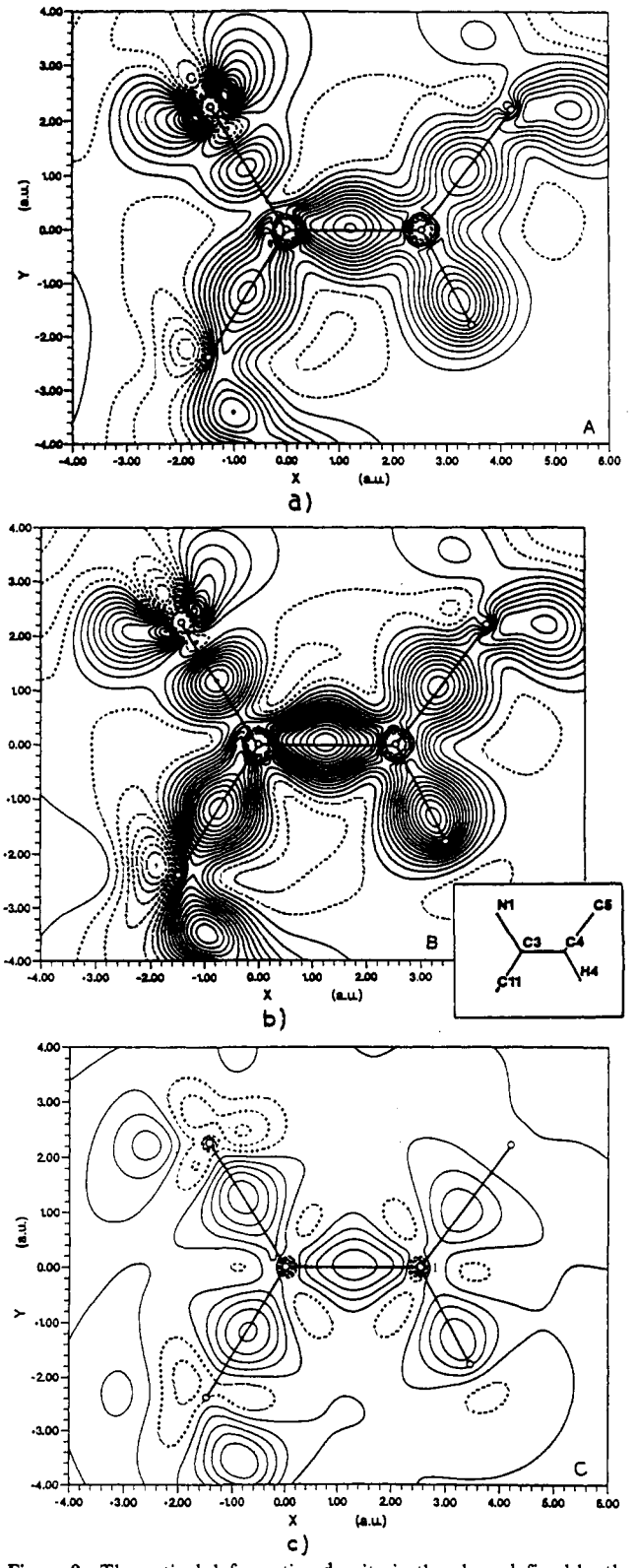

Figure 9. Theoretical deformation density in the plane defined by the atoms C_α–C_β–N_1 (see Chart I for the correspondence with working labels): basis set I (a), basis set II (b), and $\Delta(\Delta\rho) = \rho_{mol}$(basis II) – ρ_{mol}(basis I) (c). Solid lines for zero and positive contours, dotted line for negative contours; contour interval 0.05 e Å^{-3}.

lone pairs of each oxygen atom are well separated and the corresponding peak heights in the dynamic maps vary from 0.51 to 0.71 e Å^{-3} depending on their implication in intermolecular hy-

(44) Longchambon, F.; Gillier-Pandraud, H.; Wiest, R.; Rees, B.; Mitschler, A.; Feld, R.; Lehmann, M.; Becker, P. *Acta Crystallogr.* **1985**, *B41*, 47–56.

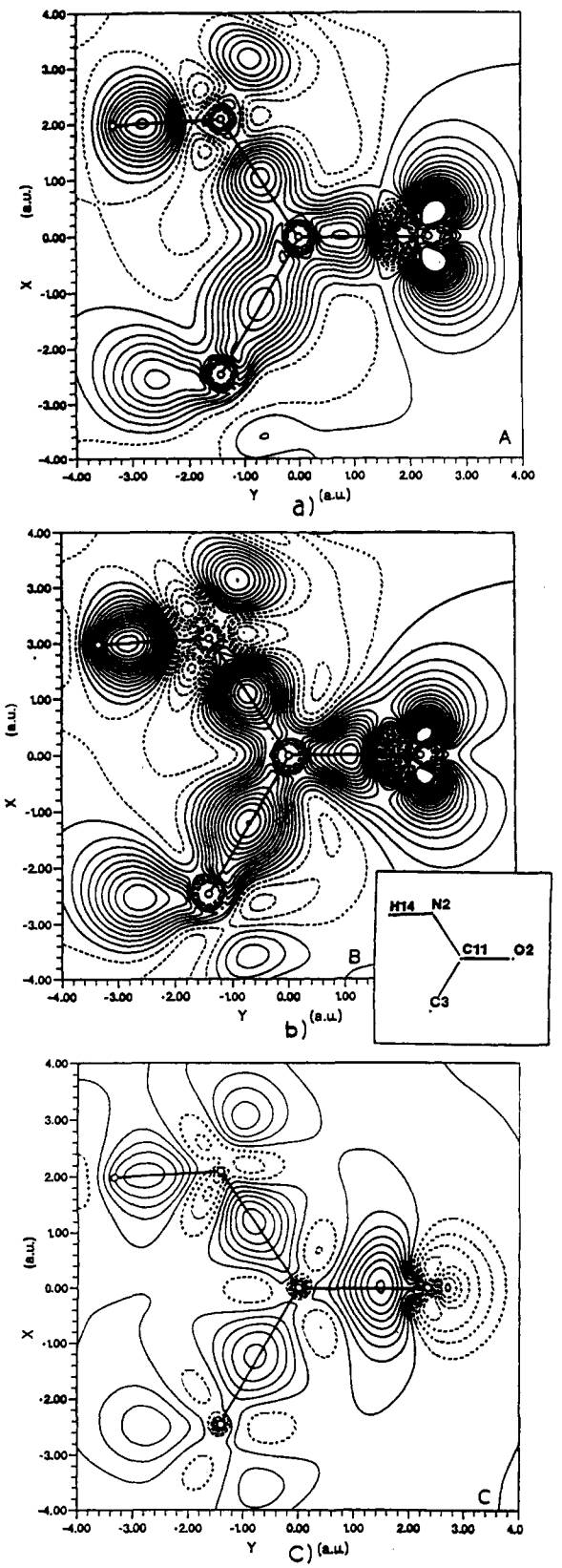

Figure 10. Theoretical deformation density in the plane defined by the atoms C_α–C′–O_1: basis set I (a), basis set II (b), and $\Delta(\Delta\rho)$ (c). Contours as in Figure 9.

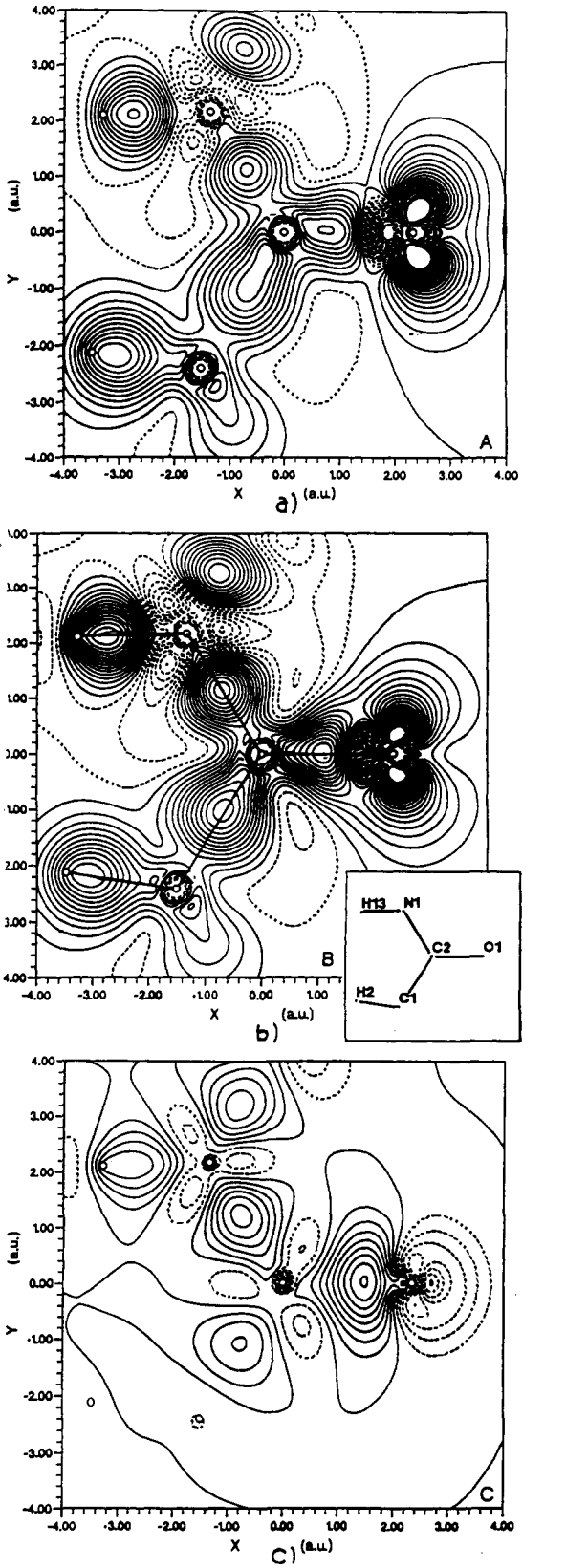

Figure 11. Theoretical deformation density in the plane defined by N_1–C'_0–O_0: basis set I (a), basis set II (b), and $\Delta(\Delta\rho)$ (c). Contours as in Figure 9.

drogen bonds. Most of the small discrepancies obtained between comparable maps from experiment and theory are consistent with those obtained in the formamide study.[39] A slight underestimation ($\sim$0.1 e Å^{-3}) on the C–O bond peak is obtained in the theoretical distribution, and experimental maps underestimate the C—H bond peaks. The present work suggests also that theory underestimates the peak height in the C_α=C_β and C=O double bonds by 0.1 e Å^{-3} and overestimates the height of the C—C single bonds (see C_3–C_{11}).

A detailed study of the basis set effects on the deformation density of CO suggests that a significant increase of the bond peak height results from the introduction of more polarization func-

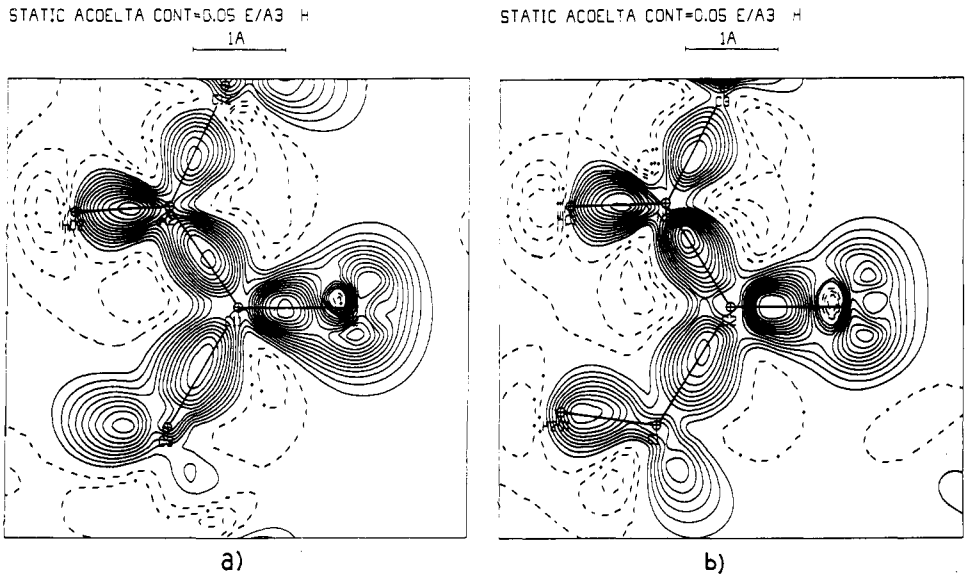

Figure 12. Crystallographic static deformation density in the planes defined by C_α–C′–O_1 (a) and by N_1–C′$_0$–O_0 (b). Contours as in Figure 2.

Table IX. Comparison of Bond Peak Heights (e Å^{-3}) and Bond Distances (Å)

type	bond	distance: uncoor	distance: corr	ρ_{exp}	ρ_{static}	ρ_{theor}[a]	ρ_{theor}[b]
C–C[d]	C_1–C_2	1.5034 (5)	1.505	0.40	0.51	0.58[c]	0.43
	C_3–C_{11}	1.5027 (7)	1.504	0.55	0.57	0.65	0.44
	C_4–C_5	1.4717 (7)	1.474	0.55	0.57	0.53[c]	0.41
C–C[e]	C_5–C_6	1.4044 (6)	1.407	0.57	0.66		0.49
	C_5–C_7	1.4010 (6)	1.403	0.57	0.66		0.49
	C_8–C_9	1.3953 (7)	1.397	0.58	0.72		0.49
	C_9–C_{10}	1.3927 (7)	1.395	0.60	0.72		0.49
	C_7–C_{10}	1.3943 (8)	1.397	0.58	0.73		0.49
	C_6–C_8	1.3917 (9)	1.394	0.59	0.74		0.49
C–C[f]	C_3–C_4	1.3473 (7)	1.348	0.73	0.82	0.74	0.56
C–N[g]	C_{11}–N_2	1.3356 (4)	1.339	0.50	0.63	0.65	0.38
	C_2–N_1	1.3470 (4)	1.351	0.50	0.64	0.64	0.37
C–N[h]	C_3–N_1	1.4118 (4)	1.413	0.37	0.47	0.50	0.27
	C_{12}–N_2	1.4484 (8)	1.450	0.35	0.39	0.41[c]	0.24
C–O	C_2–O_1	1.2383 (3)	1.242	0.56	0.69	0.65	0.41
	C_{11}–O_2	1.2387 (7)	1.241	0.61	0.73	0.65	0.41
C–H	Phenyl	1.07		0.38	0.56		0.61
	C_4–H_{104}	1.07		0.40	0.52	0.73	0.54
N–H	N_2–H_{02}	1.03		0.50	0.61	0.69	0.46
	N_1–H_{01}	1.03		0.45	0.64	0.70	0.46

[a] Calculations carried out with basis set II (triple-ζ plus polarization), except for the methyl and phenyl substituents. [b] Calculations carried out with basis set I (split valence). [c] One atom of the considered bond is described with basis set I. [d] Single C–C bonds. [e] Phenyl ring C–C bonds. [f] Double C–C bond. [g] C–N bonds with double-bond character. [h] C–N single bonds. [i] Corrected for whole-molecule and internal torsional librations (see Table VII).

tions.[35] By contrast, the correlation of the bonding electrons, neglected in the present study, brings back into the wave function some contribution from the antibonding orbital. This should therefore tend to decrease the bond accumulation. Even though relatively old investigations on N_2 and CO[45] suggest the opposite trend, as does a calculation on the N_3^- ion[46] more recent calculations[47] confirm that $\Delta\rho_{corr} = \rho_{CI} - \rho_{SCF}$ is consistently negative along all investigated bonds.[47] The correlation correction is small, however. According to Breitenstein et al.,[47] $\Delta\rho_{corr}$ varies from −0.02 e Å^{-3} in the C≡C bond of acetylene to −0.10 e Å^{-3} in F_2.

To summarize, the SCF calculations with the split-valence basis set (basis set I) provide correct positions of the density accumulation regions and of the extremes of the deformation density, but, except for the C–H bond peaks and for the lone pairs, the values of these extremes are underestimated by 30–50%. In contrast with that, the bond peak heights of the experimental static model maps are reproduced, except for C–H, within 0.1 e Å^{-3} by the SCF calculations using a basis set of triple-ζ plus polarization quality (basis set II). The remaining discrepancies are attributed to the opposing effects of basis set truncation and neglect of electron correlation. On the experimental side, the C–H discrepancy requires better hydrogen atom modeling, and an even higher resolution in sin θ/λ would reduce the observed differences on the oxygen lone pairs.

Concluding Remarks

Almost quantitative agreement is obtained between experimental static deformation maps and extended triple-ζ plus polarization theoretical maps. However, even at this level of theoretical or experimental accuracy it is not possible to draw any definitive conclusions on the effect of α, β dehydrogenation on the deformation density of the peptide bonds. The size of this effect is certainly smaller than the discrepancy between theory and experiment (0.1 e Å^{-3}). However, the different net charges observed on the peptide and C=O groups as well as the short C_3—C_{11} distances would support a higher contribution of con-

(45) Grimaldi, F.; Lecourt, A.; Moser, C. *Int. J. Quantum Chem.* **1967**, *1S*, 153.
(46) Stevens, E. D.; Rys, J.; Coppens, P. *J. Am. Chem. Soc.* **1977**, *99*, 265.
(47) (a) Breitenstein, M.; Dannohl, H.; Meyer, H.; Schweig, A.; Seeger, R.; Seeger, U.; Zittlau, W. *Int. Rev. Phys. Chem.* **1983**, *3*, 335. (b) Breitenstein, M.; Dannohl, H.; Meyer, H.; Schweig, A.; Zittlau, W. In *Electron Distributions and the Chemical Bond*; Coppens, P., Hall, M. B., Eds.; Plenum Press: New York, 1982; pp 255-281.

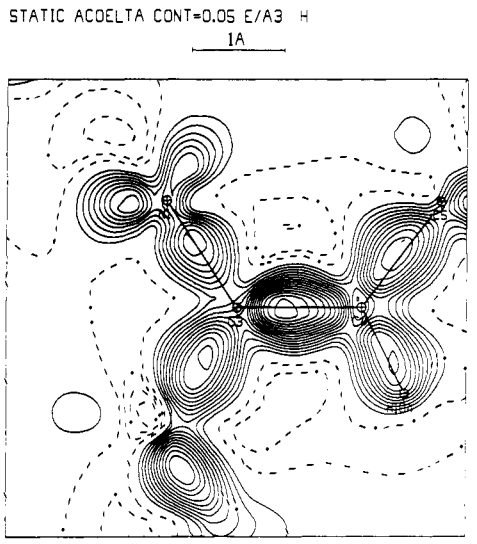

Figure 13. Crystallographic static deformation density in the plane defined by the atoms C_α-C_β-N_1. Contours as in Figure 2.

jugation Scheme 2. Anyhow the difference of reactivity between peptides and α,β-dehydrogenated pseudopeptides is certainly more related to the special molecular conformation of the side chain imposed by the C_α=C_β double bond rather than to electronic effects. Very recent results of Souhassou and Li[48] indicate that whereas the α,β-dehydrogenation and conjugation effects are not visible in the deformation density maps, the effects can be seen clearly in a topological analysis of the gradient vector paths and the Laplacian of the total electron density using the methods of Bader and his co-workers.[49]

Acknowledgment. Support of this work by the CNRS and the University of Nancy I is gratefully acknowledged. We thank Dr. A. Aubry for fruitful discussions, and Drs. G. Boussard and M. Marraud for the generous gift of this α,β-dehydropeptide. R.H.B is grateful for support from USDHHS PHS NIH Grant GM34073. The quantum-chemical calculations were carried out with a grant for computing time of the CNRS on the IBM 30-90 of "Le centre de calcul de Strasbourg Cronenbourg"; the staff is gratefully acknowledged for this collaboration.

Registry No. *N*-AcΔPhe-NHMe, 81307-03-1.

Supplementary Material Available: Residual density maps in the C_α=C_β plane, in the N_2—C′=O_1 plane, in the benzene group, and in the N_1—C′—O_0 plane at 1.35- and 0.90-Å^{-1} resolution and deformation density maps of the benzene group and of the C_α=C_β double bond at 1.0-Å^{-1} resolution (3 pages); listing of observed and calculated structure factors and esd's (39 pages). Ordering information is given on any current masthead page.

(48) Souhassou, M.; Li, N. *American Crystallographic Meeting*, Toledo, OH, July 1991.
(49) Bader, R. F. W. *Atoms in Molecules—A Quantum Theory*; Oxford Union Press: Oxford, UK, 1990.

Theoretical Studies of the Kinetics, Thermochemistry, and Mechanism of H-Abstraction from Methanol and Ethanol

Leonardo Pardo,† Jason R. Banfelder, and Roman Osman*

Contribution from the Department of Physiology and Biophysics, Mount Sinai School of Medicine of the City University of New York, One Gustave L. Levy Place, New York, New York 10029. *Received March 4, 1991*

Abstract: The process of hydrogen abstraction from methanol and ethanol has been calculated with ab initio quantum chemical methods with extended basis sets (6-311G**) and with the inclusion of correlation up to MP4SDQ. These studies serve as a model of such processes in large molecules of biological importance including the sugar moiety of DNA. A comparison of geometries of ground and transition states optimized at UHF and MP2 levels with the 6-31G basis set shows that the UHF optimized geometries have lower energies at the highest level of theory used (MP4SDQ/6-311G**). The transition states occur at a somewhat later stage along the reaction coordinate at the UHF level than at the MP2 level. Energy barriers, along with zero-point energies, were used to calculate the rate constants for H-abstraction from C_α of methanol and ethanol. Tunneling corrections were applied according to an Eckart treatment of an unsymmetrical unidimensional barrier. The corrected rate constants are in very good agreement with experiment over a wide range of temperatures. The same approach was used to predict the rate constant for the abstraction of the hydrogen from C_β of ethanol, which is not known from experimental measurements. The calculated C–H bond strengths and heats of reactions are also in good agreement when the correlation energy is scaled according to the MPnSAC approach. The geometric and energetic parameters of the transition states behave according to Hammond's postulate, i.e., the more exothermic the H-abstraction, the closer is the transition state to the reactants. This relationship suggests that the C–H bond strength is one of the major factors that determine the barrier to H-abstraction. An analysis of the MCSCF wave function constructed from a CAS of three electrons distributed in three orbitals (σ_{CH}, σ^*_{CH}, and the orbital containing the unpaired electron) supports this conclusion.

Introduction

The severe biological consequences of exposure to ionizing radiation are attributable to the lesions it causes in essential biological molecules. DNA is one of the most important target molecules that is damaged as a result of the chemical reactions caused by ionizing radiation, because irreparable damage produced in DNA usually leads to cell death. Hydroxyl radicals (OH•) produced by ionizing radiation can lesion DNA by an indirect mechanism of hydrogen abstraction, which is followed by a β-elimination of the phosphate to produce a strand break.[1] The hydrogen abstraction from deoxyribose seems to be the critical

† Permanent address: Laboratory of Computational Medicine, Department of Biostatistics, Faculty of Medicine, Universidad Autonoma de Barcelona, 08193 Bellaterra, Barcelona, Spain.

(1) von Sonntag, C. *The Chemical Basis of Radiation Biology*; Taylor & Francis: London, 1987.

0002-7863/92/1514-2382$03.00/0